Supporting Information

Lead-free Ferroelectric $Bi_{0.5}Na_{0.5}TiO_3$ based Flexible, Lightweight Nanogenerator for Motion Monitoring Application

Nirmal Prashanth Maria Joseph Raj, Abisegapriyan KS, Gaurav Khandelwal, Nagamalleswara Rao Alluri, Sang-Jae Kim*

Mailing address:

Nirmal Prashanth Maria Joseph Raj, Abisegapriyan KS, Gaurav Khandelwal, Nagamalleswara Rao Alluri, Sang-Jae Kim*

Nanomaterials & System Lab,

Major of Mechatronics Engineering,

Faculty of Applied energy system,

Jeju National University,

Jeju 63243, South Korea.

Email ID: nirmalpm@jejunu.ac.kr, abipriyan3@jejunu.ac.kr, gaurav@jejunu.ac.kr, alluri@jejunu.ac.kr, kimsangj@jejunu.ac.kr

*Corresponding author

Measurements

The structural properties of the prepared BNT NPs analyzed using an Empyrean X-ray diffractometer by Malvern Panalytical. The Raman spectroscopy analysis performed using LabRAM by Horiba. The IM3570 impedance analyzer by Hioki was used in dielectric properties studies at room temperature (RT). The BNT system PE loop measurement was performed by Radiant Technologies (PLC21216-375) at RT. The American Piezo d_{33} Tester is used in the quantification of the piezoelectric coefficient. The morphological analysis, elemental spectrum, and mappings were performed from MIRA3 by TESCAN. The HF01-37 by Lin Mot was used in applying constant mechanical force. The applied compressive force was measured by the Force and Torque indicator from Mecmesin. The JIBT 200 by Junil Tech was used in applying bending force. The energy harvesting outputs were measured by Keithley electrometer 6514. The Piezo Force Microscopy (PFM) analyses performed from a Scanning Probe Microscope (SPM) by Multimode 8 (Bruker).

Supporting figures

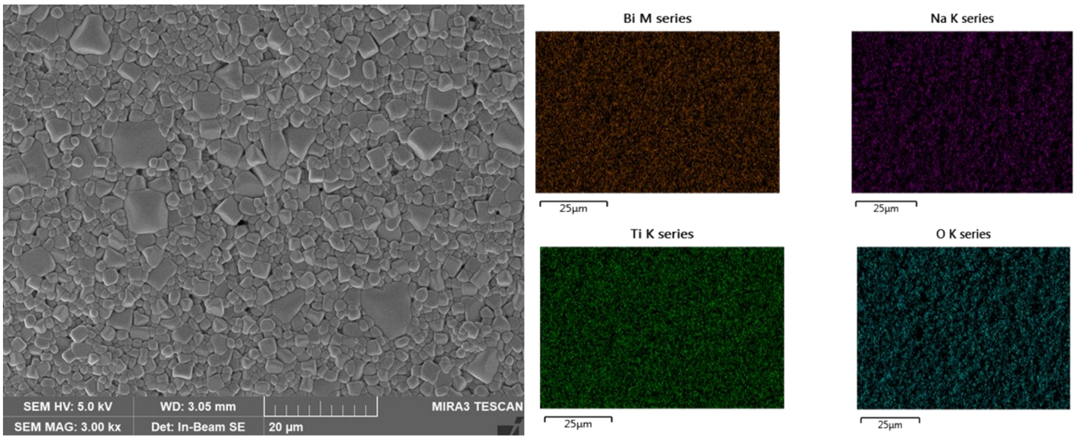

Fig.S1 The SEM image of the sintered BNT disks and it's corresponding EDS mapping images.

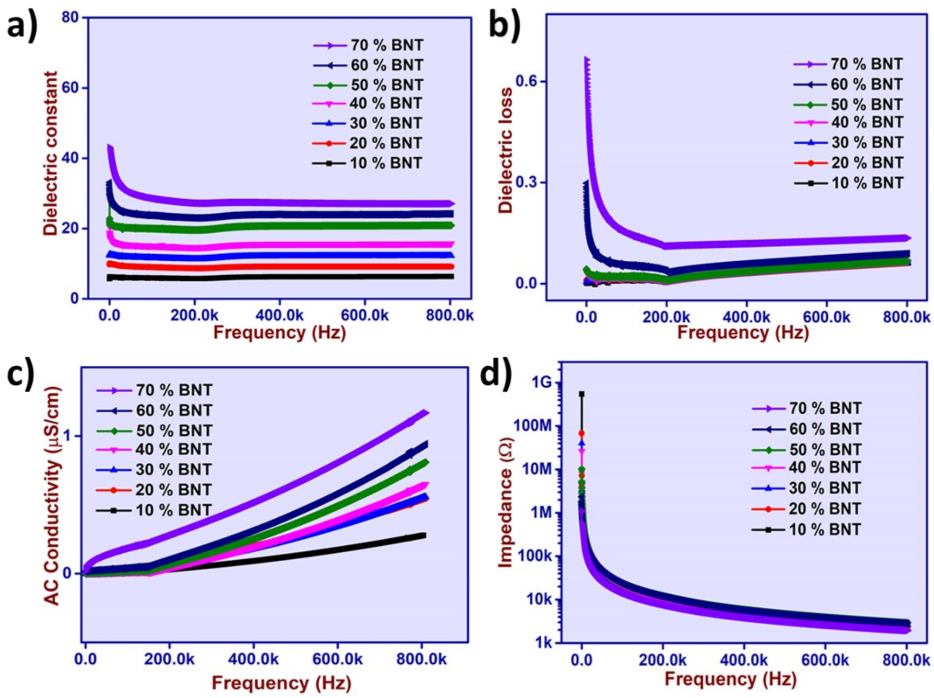

Fig.S2 The frequency-dependent dielectric studies of the prepared BNT composite films. (a) Dielectric constant, (b) Dielectric loss, (c) AC Conductivity, (d) Impedance.

PBNT composite films dielectric analysis:

The dielectric constant of the composite films increases from 6 to 28 at 100 kHz by load varying from 10 to 70 % of BNT NPs. The interfacial polarization with dipolar polarization, shown a high dielectric constant of 43 at low frequency, which later dropped to 27 at higher frequencies. The dielectric loss is one of the piezoelectric loss affecting the energy harvesting performance[1]. The initial loading of 10 to 50 % of BNT NPs shown a low dielectric loss variation from 0.003 to 0.01, but the further loading leads to a rapid increment of dielectric loss. The 60 % gave 0.04, while it reached 0.11 for 70 % at 200 kHz, and this high dielectric loss indicates the reduction in energy harvesting performance. Further, the conductivity and impedance studies performed, and it follows a similar trend of dielectric loss with the maximum conductivity of 0.27 μS/cm observed for 70 %, and low impedance of 9.42 kΩ at 200 kHz. These results indicate the 50 % loading of BNT NPs was optimum with good dielectric constant and reasonable loss, while the higher loading gives huge loss, which will affect the electrical outputs. As shown in Fig.4, the structural instability with cracks and voids at higher loading is the major reason for huge losses.

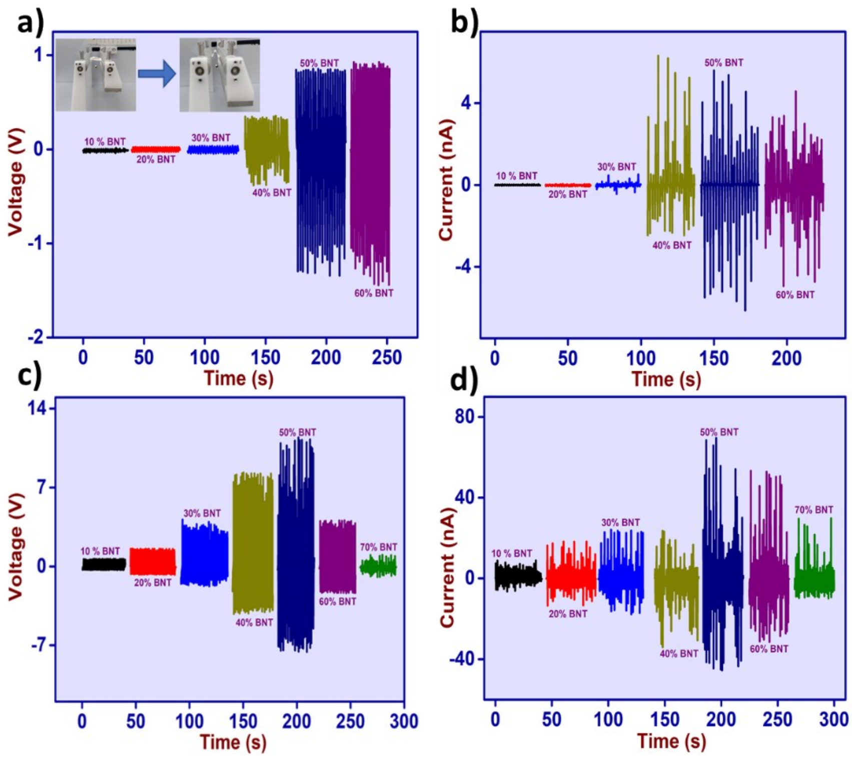

Fig.S3 (a) The voltage response of unpoled PBNT CPNGs under bending force. Inset digital images show the device in normal and bending motion conditions (Strain ~ 1.5 %). **(b)** The current response of PBNT CPNGs under bending force. **(c)** The voltage response of unpoled PBNT CPNGs under a compressive force of 6 N force @ 1 m/s^2. **(d)** The current response of unpoled PBNT CPNGs under a compressive force of 6 N force @ 1 m/s^2.

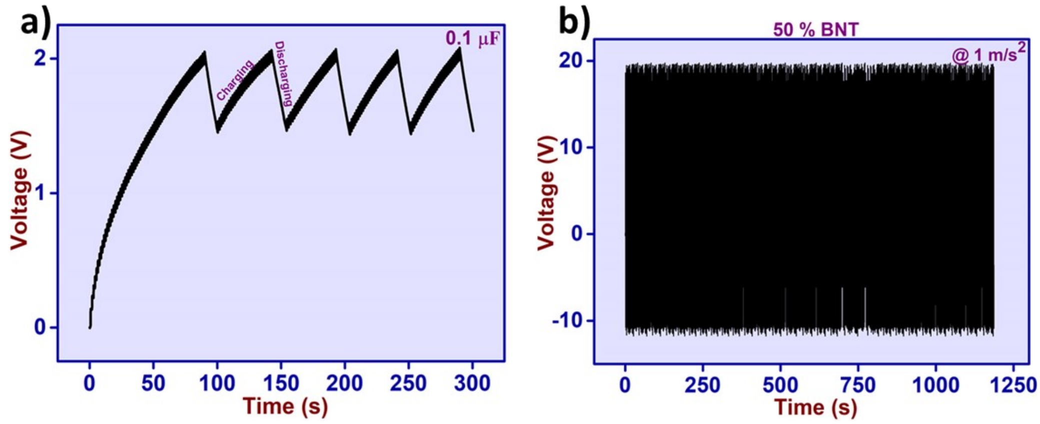

Fig.S4 (a) The charging-discharging cycle of 0.1 μF capacitors using 50 % PBNT CPNG. **(b)** The 50 % PBNT CPNG device voltage stability at 6 N force @ 1 m/s^2 for over 1000 s.

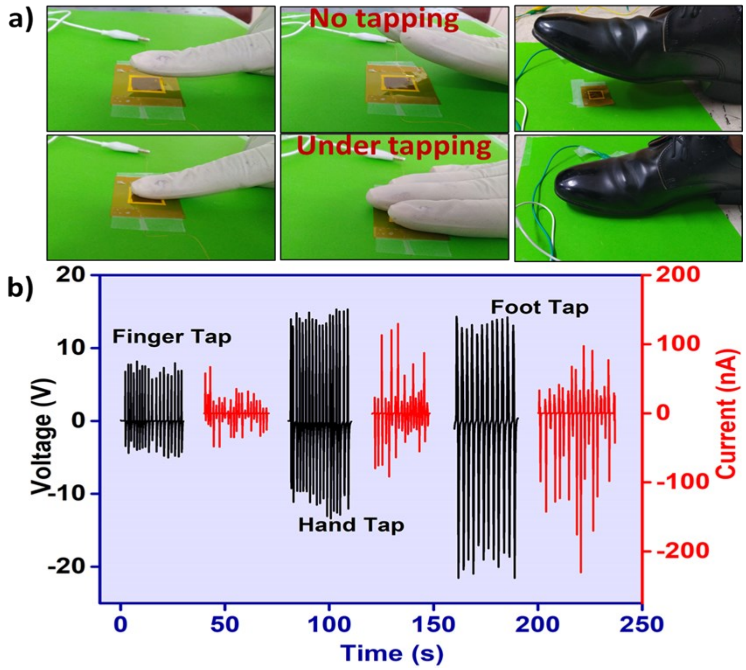

Fig.S5 The energy harvesting from biomechanical force **(a)** The force conditions under tapping and not tapping conditions. **(b)** The measured voltage and current response under tapping and no tapping conditions.

Supporting table

Table R1: Comparison table of the prepared BNT system electrical properties with the reported BNT materials.

Material	ε	ε_0	T_d (^oC)	ε_m	P_r ($\mu C/cm^2$)	E_c (kV/cm)	d_{33} (pC/N)
BNT [2]	~350 @ 100 kHz	~0.12 @100kHz	200 @ 100 kHz	2745 @ 100 kHz	38	66	-
BNT [3]	262 @ 10 kHz	0.0962 @ 10 kHz	-	-	-	-	-
BNT [4]	-	-	-	2800 @1 kHz	-	-	-
BNT [5] Unpoled	~ 410 @ 10 kHz	~ 0.05 @ 10 kHz	~ 145 @ 10 kHz	1170@ 10 kHz	32.7	65	-
BNT [5] Poled	~ 460@ 10 Hz	~ 0.05 @ 10 kHz	~ 145 @ 10 kHz	2200@ 10 kHz			
BNT [6]	~340 @100 kHz	~0.08 @100 kHz	200 @ 100 kHz	2750@ 100 kHz	~41	~61	
BNT [7]	~250 @ 1 kHz	~0.15 @ 1 kHz	~ 226 @ 1 kHz	2825 @ 1 kHz	~38	~58	-
BNT [8]	~ 340 @ 100 kHz	~ 0.02 @ 1 kHz	190 @ 100 kHz	2700 @ 100 kHz	-	-	74
BNT [9]	400 @ 1 kHz	-	190 @ 1 kHz	2900 @ 1 kHz	~ 24.3	~ 63	74
This work	338 @ 1 kHz	0.039 @ 1 kHz	206 @ 1 kHz	3035@ 1 kHz	34	60	79

ε = Dielectric constant, ε_0 = Dielectric loss, ε_m = Maximum dielectric constant, T_d = Depolarization temperature, P_r = Remanent Polarization, E_c = Coercieve field, d_{33}= Piezoelectric coeffcient.

Table S2: Comparison of energy harvesting performance of proposed work with recently published works

Active Materials	Electrode	Device Area (cm^2)	Applied force (kPa)	Voltage (V)	Current (µA)	Usage
$Bi_4Ti_3O_{12}$ [10]	Al	4	25	12.5	0.1	Force sensor
$Bi_4Ti_3O_{12}$ [10]	Al	4	Hand force	10	0.06	-
$Bi_4Ti_3O_{12}$ [11]	ITO	-	Hand force	1.6	-	-
PVDF [12]	Cu	-	15	0.7	0.083	
$BiFeO_3$ [13]	Al	1	Hand force	3	0.25	-
PVDF/ $NaNbO_3$ [12]	Cu		15	1.746	0.216	-
PVDF [14]	-	-	0.039	0.001	-	Pressure sensor
PVDF/FNC [14]	-	-	0.039	0.008	-	Pressure sensor
$0.91K_{0.48}Na_{0.52}NbO_3$-$0.04Bi_{0.5}Na_{0.5}ZrO_3$-$0.05AgSbO_3$-$0.2\%Fe_2O_3$ [15]	Cu	4	75	75	7.5	Force sensor
Mn-modified $(K_{0.5}Na_{0.5})NbO_3$ [16]	Ag	1	-	16	10	-
$(1-x)$ $KNaNbO_3$-x $BaTiO_3$ NPs [17]	ITO	9	30	55	0.410	Sleep monitoring
$K_{0.5}Na_{0.5}NbO_3$-$BaTiO_3$/PVDF [18]	Al	9	1	160	0.4	-
$Pb[Zr_{(x)}Ti_{(1-x)}]O_3$ [19]	Au	-	-	365	240	-
$Pb(Zr_{0.52}Ti_{0.48})O_3$ [20]	-	-	-	209	53	-
$Pb(Zr_{0.52}Ti_{0.48})O_3$ [21]	Au	-	-	6.5	-	-
rGO/$Pb(Mg_{1/3}Nb_{2/3})O_3$–$PbTiO_3$/PVDF-TrFe [22]	-	-	-	8.4	-	-
$Bi_{0.5}(Na_{0.6}K_{0.4})_{0.5}TiO_3$ [23]	Al/PES	4	50	11	-	-
$Bi_{0.5}(Na_{0.83}K_{0.17})_{0.5}TiO_3$ [24]	ITO	-	Finger tapping	3.5	0.28	-
$0.78Bi_{0.5}Na_{0.5}TiO_3$-$0.22SrTiO_3$ [25]	Cu IDT	2.5	-	1.31	-	Frequency sensor
$0.92(Na_{0.5}Bi_{0.5})TiO_3$-$0.04(K_{0.5}Bi_{0.5})TiO_3$-$0.04BaTiO_3$ [26]	Ag paste	-	Cantilever model	12	-	-
$Bi_{0.5}Na_{0.5}TiO_3$ (Present work)	Au	4	15 @ 1 m/s^2	22	0.14	Acceleration sensor

FNC: Fluorinated nanocellulose crystals; PES: Polyethersulfone; IDT: Interdigitated electrodes.

References:

1. A. V. Mezheritsky, *IEEE transactions on ultrasonics, ferroelectrics, and frequency control*, 2004, **51**, 695-707.
2. M. Zannen, M. Dietze, H. Khemakhem, A. Kabadou and M. Es-Souni, *Ceramics International*, 2014, **40**, 13461-13469.
3. P. Laoratanakul, R. Yimnirun and S. Wongsaenmai, *Current Applied Physics*, 2011, **11**, S161-S166.
4. K. Hao, W. Ge, Z. Ren, X. Liu, L. Luo, X. Li, H. Luo and D. Viehland, *Journal of the American Ceramic Society*, 2020, **103**, 3349-3360.
5. K. R. Kandula, S. Asthana and S. S. K. Raavi, *RSC Advances*, 2018, **8**, 15282-15289.
6. M. Benyoussef, M. Zannen, J. Belhadi, B. Manoun, J.-L. Dellis, M. El Marssi and A. Lahmar, *Ceramics International*, 2018, **44**, 19451-19460.
7. M. Zannen, A. Lahmar, Z. Kutnjak, J. Belhadi, H. Khemakhem and M. El Marssi, *Solid State Sciences*, 2017, **66**, 31-37.
8. Y. Sung, J. Kim, J. Cho, T. Song, M. Kim, H. Chong, T. Park, D. Do and S. Kim, *Applied Physics Letters*, 2010, **96**, 022901.
9. D. J. Ruth and B. Sundarakannan, *Journal of Materials Science: Materials in Electronics*, 2016, **27**, 3250-3257.
10. N. P. M. J. Raj, N. R. Alluri, G. Khandelwal and S.-J. Kim, *Composites Part B: Engineering*, 2019, **161**, 608-616.
11. N. Abinnas, P. Baskaran, S. Harish, R. S. Ganesh, M. Navaneethan, K. Nisha, S. Ponnusamy, C. Muthamizhchelvan, H. Ikeda and Y. Hayakawa, *Applied Surface Science*, 2017, **418**, 362-368.
12. H. H. Singh, S. Singh, N. J. C. S. Khare and Technology, 2017, **149**, 127-133.
13. X. Ren, H. Fan, Y. Zhao and Z. Liu, *ACS applied materials & interfaces*, 2016, **8**, 26190-26197.
14. F. Ram, A. Gudadhe, T. Vijayakanth, S. Aherrao, V. Borkar, R. Boomishankar and K. Shanmuganathan, *ACS Applied Polymer Materials*, 2020.
15. M. Wu, T. Zheng, H. Zheng, J. Li, W. Wang, M. Zhu, F. Li, G. Yue, Y. Gu and J. Wu, *Journal of Materials Chemistry A*, 2018, **6**, 16439-16449.
16. M. Zheng, Y. Hou, X. Yan, L. Zhang and M. Zhu, *Journal of Materials Chemistry C*, 2017, **5**, 7862-7870.
17. V. Vivekananthan, A. Chandrasekhar, N. R. Alluri, Y. Purusothaman, W. J. Kim, C.-N. Kang and S.-J. Kim, *Materials Letters*, 2019, **249**, 73-76.
18. V. Vivekananthan, N. R. Alluri, Y. Purusothaman, A. Chandrasekhar and S.-J. Kim, *Nanoscale*, 2017, **9**, 15122-15130.
19. K. I. Park, J. H. Son, G. T. Hwang, C. K. Jeong, J. Ryu, M. Koo, I. Choi, S. H. Lee, M. Byun and Z. L. Wang, *Advanced materials*, 2014, **26**, 2514-2520.
20. L. Gu, N. Cui, L. Cheng, Q. Xu, S. Bai, M. Yuan, W. Wu, J. Liu, Y. Zhao and F. Ma, *Nano letters*, 2013, **13**, 91-94.
21. W. Jin, Z. Wang, H. Huang, X. Hu, Y. He, M. Li, L. Li, Y. Gao, Y. Hu and H. Gu, *RSC advances*, 2018, **8**, 7422-7427.
22. J. Kim, J.-H. Ji, D.-J. Shin, S. Yoon, Y.-H. Ko, K.-H. Cho and J.-H. Koh, *Applied Surface Science*, 2019, **494**, 1000-1006.
23. K. Batra, N. Sinha and B. Kumar, *Journal of Materials Science: Materials in Electronics*, 2019, **30**, 6157-6165.
24. Q. Yang, D. Wang, M. Zhang, T. Gao, H. Xue, Z. Wang and Z. Xiong, *Journal of Alloys and Compounds*, 2016, **688**, 1066-1071.

25. S. H. Ji, J. H. Cho, Y. H. Jeong, J.-H. Paik, J. Do Yun and J. S. Yun, *Sensors and Actuators A: Physical*, 2016, **247**, 316-322.
26. Y. Zhang, X. Liu, G. Wang, Y. Li, S. Zhang, D. Wang and H. Sun, *Journal of Alloys and Compounds*, 2020, **825**, 154020.